14th International Stellarator Workshop, September 22 - 26, 2003, Greifswald, Germany

Marginal stability diagrams for infinite-n ballooning modes in quasi-symmetric stellarators

S.R.Hudson[1], C.C.Hegna[2], R.Torasso[3] & A.Ware[4]

1) Princeton Plasma Physics Laboratory, PO Box 451, Princeton NJ 08543, USA.
2) Department of Physics, University of Wisconsin-Madison, Madison WI 53706, USA.
3) Courant Institute of Mathematical Sciences, New York University, NY 10012, USA.
4) Department of Physics and Astronomy, The University of Montana, MT 59812, USA.

Abstract

By perturbing the pressure and rotational-transform profiles at a selected surface in a given equilibrium, and by inducing a coordinate variation such that the perturbed state is in equilibrium, a family of magnetohydrodynamic equilibria local to the surface and parameterized by the pressure gradient and shear is constructed for arbitrary stellarator geometry. The geometry of the surface is not changed. The perturbed equilibria are analyzed for infinite-n ballooning stability and marginal stability diagrams are constructed that are analogous to the (s, α) diagrams constructed for axi-symmetric configurations.

The method describes how pressure and rotational-transform gradients influence the local shear, which in turn influences the ballooning stability. Stability diagrams for the quasi-axially-symmetric NCSX, a quasi-poloidally-symmetric configuration and the quasi-helically-symmetric HSX are presented. Regions of second-stability are observed in both NCSX and the quasi-poloidal configuration, whereas no second stable region is observed for the quasi-helically symmetric device.

To explain the different regions of stability, the curvature and local shear of the quasi-poloidal configuration are analyzed. The results are seemingly consistent with the simple explanation: ballooning instability results when the local shear is small in regions of bad curvature. Examples will be given that show that the structure, and stability, of the ballooning mode is determined by the structure of the potential function arising in the Schrödinger form of the ballooning equation.

1. Introduction

By employing the standard WKB-like formulation, the leading order stability of high-k ideal modes in stellarator plasmas is governed by an ordinary differential equation, the ballooning equation [1]. The ballooning equation shows that it is the interaction of pressure gradients, curvatures and the local shear that determines ballooning stability.

The local pressure gradient at a given surface directly affects the ballooning stability. A cursory investigation of ballooning stability suggests that, as the magnitude of pressure gradient is increased, ballooning modes could only be destabilized. This however is not the case. The local shear also influences ballooning stability, and the local shear is related to the pressure gradient through the Pfirsh-Schlüter currents. As the pressure gradient is increased at a given surface with fixed geometry, the local shear must change to preserve the magnetohydrodynamic (MHD) equilibrium condition. Depending on the geometry of the surface, it may be the case that the local shear will be altered in such a manner to stabilize infinite-n ballooning modes. This effect has been studied in axisymmetric equilibria [2] and may be called 'second-stability'.

In addition to this effect, as the ratio of averaged plasma energy to averaged magnetic energy, β, is increased the global equilibrium properties will be modified. For example,

as β is increased, geometrical deformations associated with the Shafranov shift will alter the curvature. This in turn will alter the ballooning stability properties.

The primary interest of this article is to examine the phenomena of second stability in stellarator geometry. Hegna & Nakajima [3] extended the method of profile variations introduced by Greene & Chance [2] to stellarator geometry. This method allows the pressure gradient to change at a given surface, but keeps the surface geometry unchanged. The MHD equilibrium condition is used to determine the self-consistent change in the local shear. This technique allows the variations in ballooning stability caused by variations in the local shear to be distinguished from the variations in ballooning stability caused by the geometrical change associated with increasing β.

2. Profile Variations

This section will outline the method of profile variations in stellarator geometry. For full details the reader is referred to Hegna & Nakajima [3]. Further discussion and details of the numerical implementation is given by Hudson & Hegna [4]. The magnetic field is given in Boozer coordinates [5]

$$\mathbf{B} = \nabla\psi \times \nabla\theta + \iota(\psi)\nabla\zeta \times \nabla\psi = h(\psi,\theta,\zeta)\boldsymbol{\nabla}\psi + I(\psi)\boldsymbol{\nabla}\theta + G(\psi)\boldsymbol{\nabla}\zeta. \tag{1}$$

For the contravariant and covariant forms to be equivalent, there are several metric identities that must be satisfied. One such identity is obtained by taking the dot product of the two forms for $\mathbf{B}$: the coordinate Jacobian must satisfy $\sqrt{g} = (G + \iota I)/B^2$. Such metric identities, and the equilibrium condition $\nabla p = \mathbf{J} \times \mathbf{B}$, are used to derive consistency relations among varied quantities.

Given such a representation for the field, it is then the coordinate transformation $\mathbf{x}(\psi,\theta,\zeta)$ itself that determines that MHD equilibrium. The method of profile variations will impose a variation in the pressure and rotational-transform profiles, and calculate the coordinate response required to preserve the MHD equilibrium condition.

The pressure and rotational-transform profiles are described in the vicinity of a selected magnetic surface ψ_b by the expansion

$$p(\psi) = p^{(0)}(\psi) + \mu p^{(1)}(y) + \ldots, \qquad \iota(\psi) = \iota^{(0)}(\psi) + \mu\,\iota^{(1)}(y) + \ldots, \tag{2}$$

where $p^{(0)}$ and $\iota^{(0)}$ are the pressure and rotational-transform profiles of the undisturbed equilibrium, $p^{(1)}$ and $\iota^{(1)}$ are the perturbation profiles, and $\mu \ll 1$ is a small expansion parameter. The auxiliary variable $y = (\psi - \psi_b)/\mu$ is used to ensure that the variations in the gradients of the pressure and rotational-transform are of lower order than the variations in the pressure and rotational-transform. The gradients of the pressure and rotational-transform take the form

$$p'(\psi) = p^{(0)\prime}(\psi) + p^{(1)\prime}(y) + \ldots, \qquad \iota'(\psi) = \iota^{(0)\prime}(\psi) + \iota^{(1)\prime}(y) + \ldots, \tag{3}$$

The coordinate transformation is similarly perturbed

$$\mathbf{x}(\psi,\theta,\zeta) = \mathbf{x}^{(0)}(\psi,\theta,\zeta) + \mu\mathbf{x}^{(1)}(y,\theta,\zeta) + \ldots \tag{4}$$

The perturbed basis vectors are

$$\mathbf{e}_\psi = \mathbf{e}_\psi^{(0)} + \partial_y\mathbf{x}^{(1)} + \ldots \qquad \mathbf{e}_\theta = \mathbf{e}_\theta^{(0)} + \mu\partial_\theta\mathbf{x}^{(1)} + \ldots \qquad \mathbf{e}_\zeta = \mathbf{e}_\zeta^{(0)} + \mu\partial_\zeta\mathbf{x}^{(1)} + \ldots, \tag{5}$$

For consistency, both G and I are perturbed similarly to p and ι, but h requires order unity variations. The lowest order quantity in the coordinate variation is $\partial_y\mathbf{x}^{(1)}$. This quantity can be expanded in the following basis set

$$\frac{\partial\mathbf{x}^{(1)}}{\partial y} = C\mathbf{B} + D\frac{\mathbf{B}\times\boldsymbol{\nabla}\psi}{B^2} + M\frac{\boldsymbol{\nabla}\psi}{g^{\psi\psi}}, \tag{6}$$

where C, D and M are to be determined. An expression for C is obtained from the momentum balance equation. By requiring that the magnetic field strength is undisturbed to lowest order gives the condition $M = 0$. An equation for the term D can be obtained, and solved numerically for a given equilibrium, from the lowest order perturbed momentum balance equation and Ampere's law

$$\partial_\eta D = \iota^{(1)\prime} \frac{1}{\oint 1/g^{\psi\psi}} \left(\frac{1}{g^{\psi\psi}} - \oint \frac{1}{g^{\psi\psi}} \right) - p^{(1)\prime} \frac{V'(G + \iota I)}{\oint 1/g^{\psi\psi}} \left(\frac{\lambda}{g^{\psi\psi}} \oint \frac{1}{g^{\psi\psi}} - \frac{1}{g^{\psi\psi}} \oint \frac{\lambda}{g^{\psi\psi}} \right), \quad (7)$$

where $\partial_\eta = \partial_\zeta + \iota \partial_\theta$, λ is related to the Pfirsh-Schlüter currents, and $4\pi^2 \oint q \equiv \oint\oint q \, d\theta d\zeta$ is the flux surface average. The function D depends on the original equilibrium: more precisely, the terms multiplying $\iota^{(1)\prime}$ and $p^{(1)\prime}$ depend only the selected surface of the original equilibrium. Once these terms have been computed, a simple task given the Fourier representation of the equilibrium, no further equilibrium calculations are required.

As far as the infinite-n ballooning equation is concerned, the only quantity which is affected by the profile variations, in addition to p' and ι', is the local shear, $s \equiv (\mathbf{b} \times \mathbf{n}) \cdot \nabla \times (\mathbf{b} \times \mathbf{n})$ where $\mathbf{b}$ and $\mathbf{n}$ are respectively the unit vectors along the magnetic field and normal to the magnetic surface. We can separate the contributions to s into a flux surface averaged quantity, the global shear ι', and the variation of the local shear, $\tilde{s}$. The quantity D describes the variation in local shear due to changes in the two profile quantities. The perturbed part of the local shear takes the simple form

$$\left(G \partial_y \mathbf{x}^{(1)} \cdot \mathbf{e}_\theta - I \partial_y \mathbf{x}^{(1)} \cdot \mathbf{e}_\zeta \right) / \left(\sqrt{g} g^{\psi\psi} \right) = D. \quad (8)$$

The term D thus represents how the profile variations affect the local shear.

The ballooning mode equation in the perturbed equilibrium is written by transforming the angle variables $\alpha = \theta - \iota\zeta, \eta = \zeta$ so that α labels the field line, η labels position along the field line and the $\mathbf{B} \cdot \nabla$ operator becomes $\mathbf{B} \cdot \nabla = \sqrt{g}^{-1} \partial_\eta$. The ballooning equation is given in a form that highlights the role of the (integrated) local shear

$$\frac{\partial}{\partial \eta} \Lambda \frac{\partial}{\partial \eta} \xi + 2(p^{(0)\prime} + p^{(1)\prime}) \sqrt{g} (G + \iota I)(\kappa_n + \kappa_g L) \xi = \omega^2(\psi, \alpha, \eta_k) \Lambda \xi, \quad (9)$$

where $\Lambda = \left(B^2 / g^{\psi\psi} + g^{\psi\psi} L^2 \right)$, L is the integrated local shear $L = \int_{\eta_k}^{\eta} d\eta' s(\eta')$, η_k is the ballooning angle and ω^2 is the ballooning eigenvalue which in general depends on the surface, field line and ballooning angle η_k (this article will only consider the case $\alpha = \eta_k = 0$). This is an ordinary differential equation with boundary condition $\xi(\pm\infty) = 0$. For numerical work, the boundary condition is that $\xi(\pm\eta_\infty) = 0$ where η_∞ is chosen to sufficiently large to contain the mode. The ballooning equation may be written in Schrödinger form $[d^2/d\vartheta^2 + E - V]\Lambda^{1/2}\xi = 0$ where the 'potential' $V(\vartheta)$ depends on the coefficients of the ballooning equation [6]. The structure of the Schrödinger potential influences the structure of the eigenvector.

The profile variations describe the separate effects that the variation in p' and ι' have on the local shear, and thus on ballooning stability. Taking p' and ι' as independent variables, a two-dimensional family of equilibrium surfaces may be constructed from a single numerically computed (VMEC) equilibrium. The ballooning stability may be determined for each of the perturbed equilibria and marginal stability curves constructed. Note that if the analysis of the perturbed equilibrium is local to the original surface ψ_b, as infinite-n ballooning analysis indeed is, then the equations describing how the variations affect the local shear are exact. Variations of any magnitude are allowed and the stability properties of the perturbed equilibria are characteristic of the geometry of the original surface.

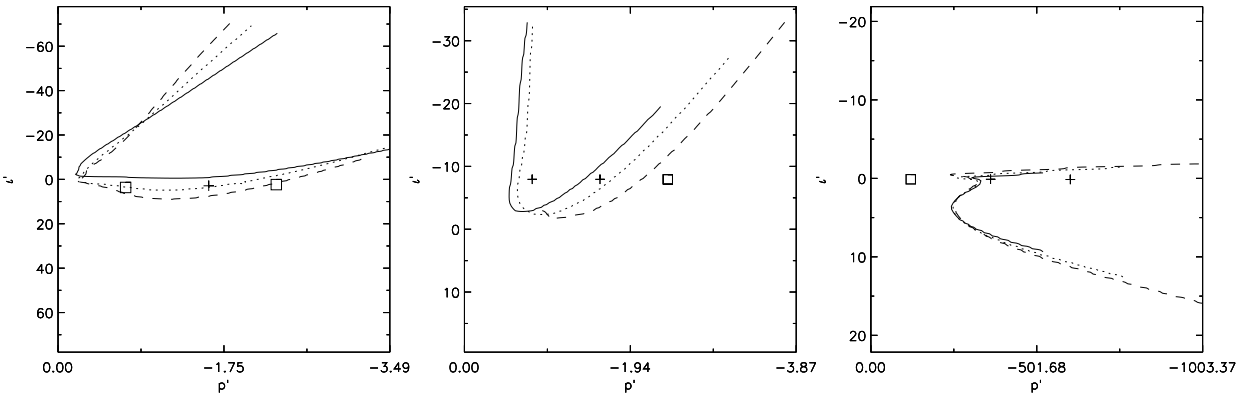

Fig. 1: Marginal stability diagrams for : (left) $li383$ VMEC surface $s = 0.6$: $\beta = 4.2\%$ (solid), $\beta = 9.5\%$ (dotted) and $\beta = 14.0\%$ (dashed); (center) $m3b15$ VMEC surface $s = 0.3$: $\beta = 1.2\%$ (solid), $\beta = 2.4\%$ (dotted) and $\beta = 3.7\%$ (dashed); (right) $hsxstd$ VMEC surface $s = 0.6$: $\beta = 0.7\%$ (solid), $\beta = 2.2\%$ (dotted) and $\beta = 3.6\%$ (dashed). Each stability diagrams is centered on the original surface, the location of which is shown with '+' if the surface is unstable and '□' if that surface is stable.

3. Stability diagrams, local shear and curvature

In Fig.(1) are shown the stability diagrams for the NCSX [7] configuration $li383$, the quasi-poloidal configuration $m3b15$ [8] and the HSX standard configuration [9] $hsxstd$. This selection reflects the current US interest in quasi-symmetric devices.

As predicted by Hegna & Hudson [10], the quasi-helically-symmetric configuration $hsxstd$ does not display a second stable region. The quasi-axisymmetric configuration $li383$ does display a second stable region, but it is quite weak in the sense that very high $\beta \approx 16\%$ is required to access this region. The quasi-poloidal-symmetric configuration $m3b15$ shows a strong second stable region as observed by Ware et al. [8].

For all of the configurations, as β is increased, there is some change in the stability diagrams. This assumedly is the result of geometric distortions of the surfaces. Nonetheless, it has been confirmed that the stability diagrams give a reasonable quantitative prediction of the marginal β limit and the qualitative agreement is very good.

To analyze the physical cause of ballooning instability, and the mechanism leading to second stability, the $m3b15$ $\beta = 2.4\%$ configuration is analyzed in some detail. Evidence is presented that is consistent with the suggestion that ballooning instability results when regions of small shear coincide with regions of bad curvature. Variations in the pressure gradient at the $s = 0.3$ VMEC surface of the $m3b15$ equilibrium at $\beta = 2.4\%$ have been imposed and the resulting configurations have been analyzed. The normal curvature for this case is shown in Fig.(2). The shear for three cases, with $(\iota^{(1)\prime}, p^{(1)\prime})$=$(0.0, 1.502)$, $(0.0, 0.404)$ and $(0.0, -0.694)$ are shown in Fig.(3). These variations in the pressure gradient place the perturbed equilibria in the first stable, unstable and second stable regions respectively for the choice $\alpha = \eta_k = 0$. Clearly the local shear is affected by the profile variations. For the second stable case, it appears that the small local shear region no longer coincides with the unfavorable curvature region.

To examine more closely the correlation between the local shear, the curvature and the structure of the eigenvector, these quantities are shown as functions along the field line for the three cases in Fig.(4). The variations in the local shear alter the correlation between regions of small local shear and bad curvature: increased pressure gradient can be stabilizing!

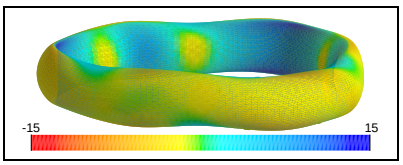

Fig. 2: (color) Normal curvature for $m3b15$ $\beta = 2.4\%$ on VMEC surface $s = 0.3$.

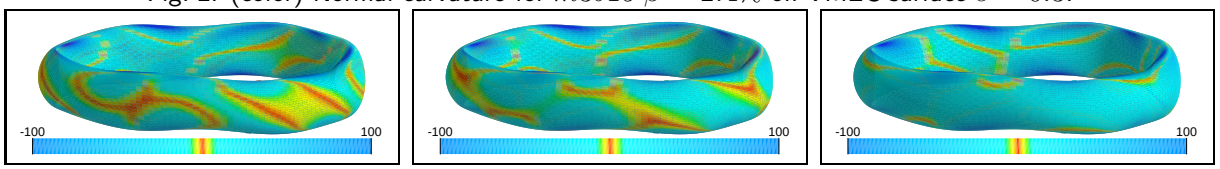

Fig. 3: (color) Local shear for $m3b15$ $\beta = 2.4\%$ on VMEC surface $s = 0.3$ with the following variations in shear and pressure gradient : (a) $(\iota^{(1)\prime}, p^{(1)\prime})$=$(0.0, 1.502)$ (left); (b) $(0.0, 0.404)$ (center); (c) $(0.0, -0.694)$ (right). Regions of small local shear are indicated with red.

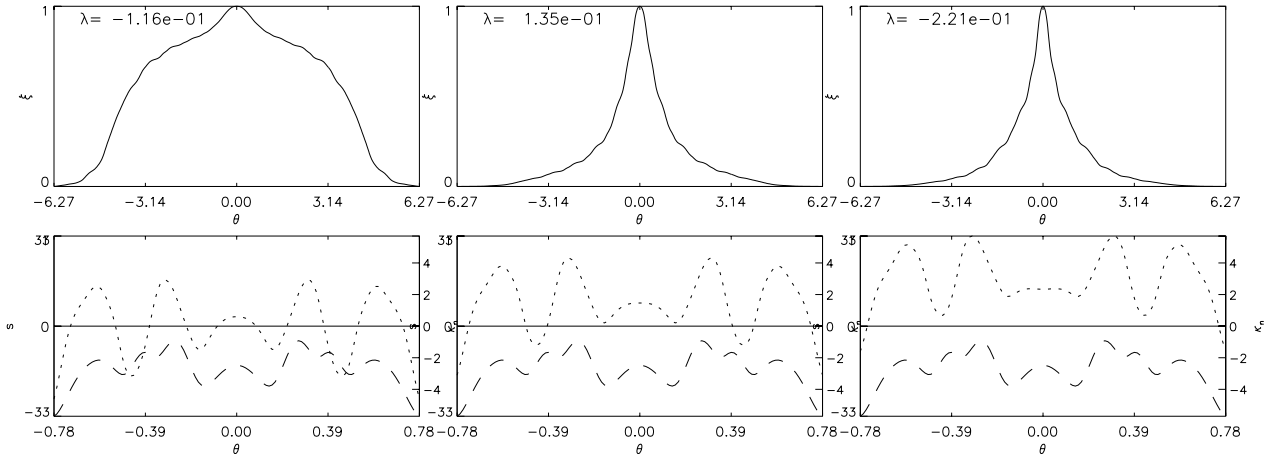

Fig. 4: Eigenvectors, local shear and normal curvature along a field line for $m3b15$ $\beta = 2.4\%$ on VMEC surface $s = 0.3$. The upper figures show the eigenvector structure over the range $[-2\pi, 2\pi]$ for $(\iota^{(1)\prime}, p^{(1)\prime})$=$(0.0, 1.502)$ (left), $(0.0, 0.404)$ (center), $(0.0, -0.694)$ (right). The lower figures show the local shear (dotted) and curvature (dashed) for each case near where the eigenvector peaks. The eigenvector seems to localize when small local shear coincides with negative curvature.

To further illustrate the effect of the pressure gradient variation, the structure of the Schrödinger potential for the three cases is shown in Fig.(5). The pressure gradient variations affect the magnitude of the peaks in the potential function. The higher the peaks, the greater the chance the mode will localize.

What is called the first stable region here for the $m3b15$ $\beta = 2.4\%$ $s = 0.3$ case may only be the first stable region for the choice $\alpha = \eta_k = 0$. From inspection of Fig.(3)a, other field lines may exist for which regions of small local shear and bad curvature coincide.

The $li383$ and $hsxstd$ configurations have been similarly analyzed. $li383$ displayed behavior similar to the $m3b15$ results presented here, including a second stable region [4]. The $hsxstd$ configuration in contrast does not display second stability. As the pressure gradient is increased, the peaks in the Schrödinger potential for $hsxstd$ seem to increase.

4. Conclusion

The method of profile variations is a efficient means to determine the stability of a family equilibria nearby a numerically computed equilibrium. It provides a good qualitative understanding and prediction of the stability properties that are characteristic of the

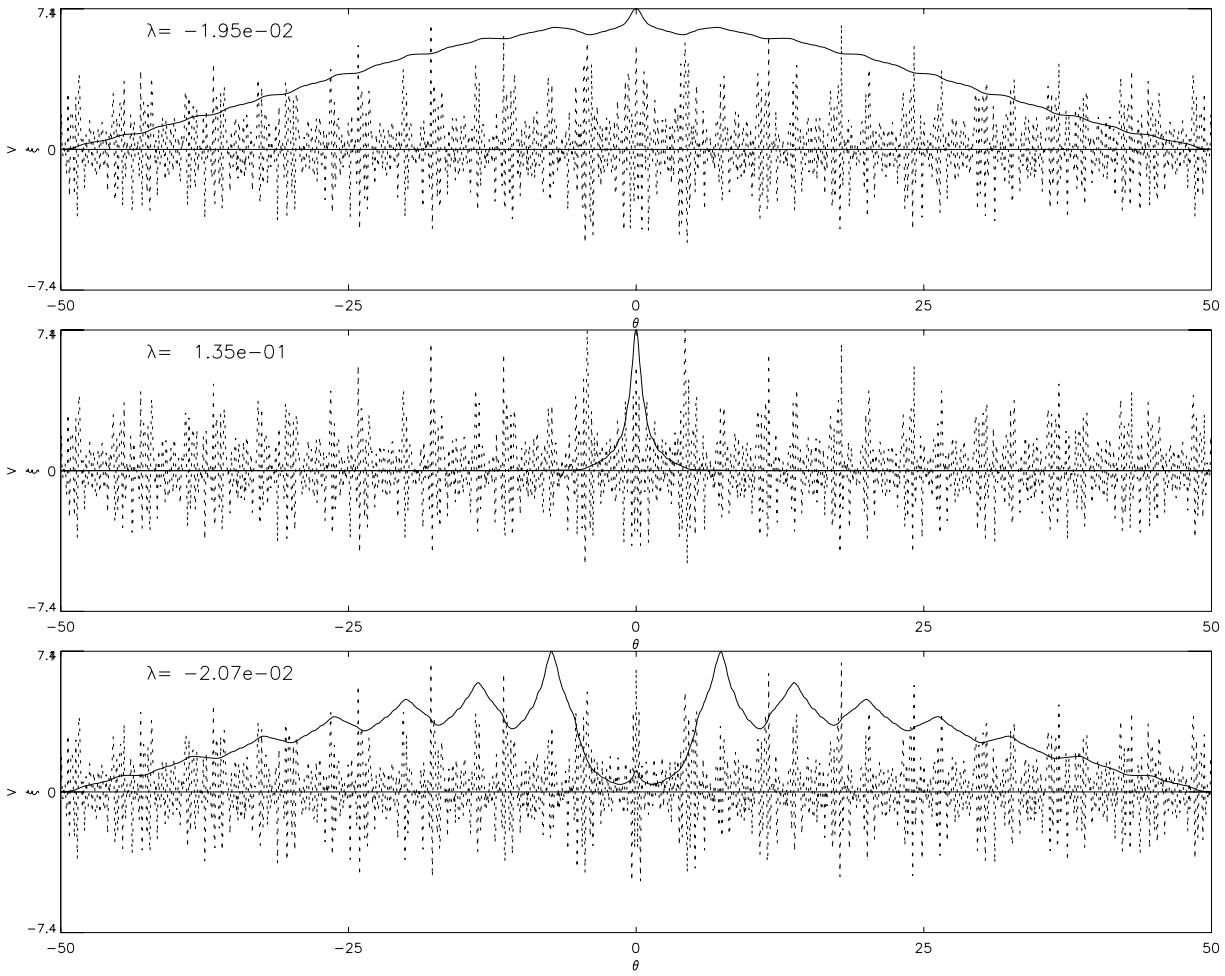

Fig. 5: Schrödinger potential (dashed) and eigenvector (solid) for $m3b15$ $\beta = 2.4\%$ on VMEC surface $s = 0.3$ configuration for $(\iota^{(1)\prime}, p^{(1)\prime})$=$(0.0, 1.502)$ (upper), $(0.0, 0.404)$ (middle) and $(0.0, -0.694)$ (lower).

geometry of the equilibrium. The quantitative agreement between predicted stability boundaries is good, but as pressure is increased global equilibrium effects can alter the geometry of the configuration: an effect not incorporated into the profile variation method.

The observations are consistent with the suggestion that ballooning modes will localize in regions of small local shear and bad curvature. Variations in the pressure gradient will alter the local shear, and thus change the where the local shear is small. In some cases, this can lead to stabilization of ballooning modes as pressure is increased.

---

[1] R.L. Dewar and A.H. Glasser. *Phys. Fluids.*, 26(10):3038, 1983.

[2] J.M. Greene and M.S. Chance. *Nucl. Fus.*, 21(4):453, 1981.

[3] C.C. Hegna and N. Nakajima. *Phys. Plasmas*, 5(5):1336, 1998.

[4] S.R.Hudson and C.C. Hegna. *Phys. Plasmas*, 2003.

[5] A.H. Boozer, *Phys. Fluids*, 25(3):520, 1982.

[6] P.Cuthbert and R.L.Dewar, *Phys. Plasmas*, 7(6):2302, 2000.

[7] M.C.Zarnstorff et al. *Plasma Physics and Controlled Fusion*,43:A237,2001.

[8] A.S.Ware et al. *Physical Review Letters*, 89(12):125003-1, 2002.

[9] J.N.Talmadge and W.A.Cooper *Physics of Plasmas*, 3(10):3713,1996.

[10] C.C.Hegna and S.R.Hudson *Physics of Plasmas*, 9(5):2014,2002.